sPHENIX Report

**tag:** sPH-INTT-2025-001-AN
**version:** 0.1
**DOI:** unspecified
**date:** May 8, 2025

# INTT Beam Test Analysis Note

Cheng-Wei Shih (editor of this analysis note), and the sPHENIX INTT group

Abstract

The analysis note for the INTT beam test conducted in ELPH in the year 2021. The analysis note coverages (1) energy deposit distribution, (2) residual distribution comparison with MC, (3) hit detection efficiency, and (4) the number of tracks compared with MC.

# 1 Important

The approval presentation for beam test analysis for publication: https://indico.bnl.gov/event/28070/#1-approval-presentation-for-be.

# 2 Introduction

For a detailed description of the setup of the INTT beam test in ELPH, please refer to https://www.raris.tohoku.ac.jp/wp-content/uploads/2025/03/ELPH_ann_rep2021.pdf. The drawing of the setup and coordination used in the beam test is shown in Figure 1. In the beam test, the Y axis of used coordination is effectively equivalent to the $\phi$ direction in 1008-IR.

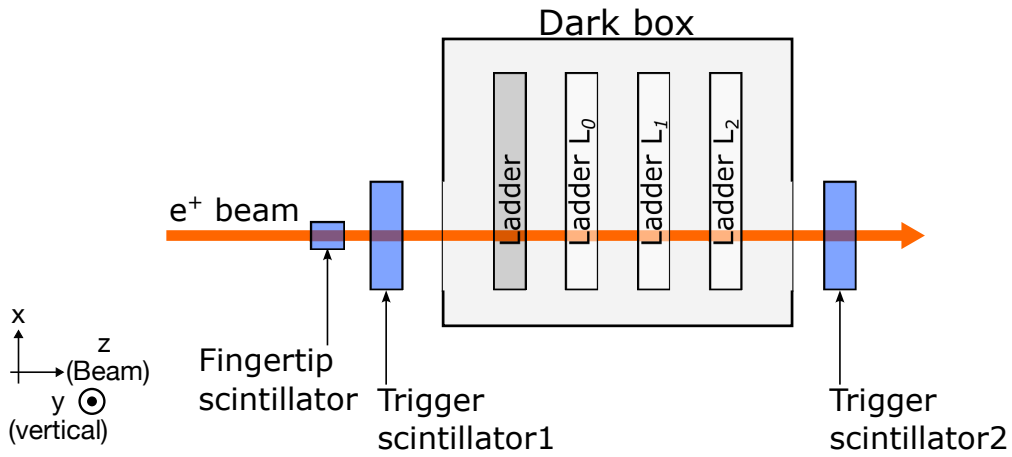


**Figure 1:** The setup for the beam test experiment at ELPH. The dark box, which contained the INTT ladders inside, was installed on the positron beam line. Two trigger scintillators and a fingertip scintillator were set upstream and downstream of the dark box. The x-, y-, and z-axes are also shown.

A summary of the beam test is listed below:

- Positron beam with the energy of 800 MeV was delivered by the ELPH facility
- Due to the good timing resolution of INTT ladder, relatively low beam intensity, and good control of the beam quality, the number of positrons interacts with INTT ladders in one INTT event (1 BCO) is assumed to be 1.
- A telescope made of four layers of the INTT ladder
  - 3 out of 4 ladders were functional (**the first ladder was deactivated due to the light leakage.**)
  - Bias voltage 50V was applied (**The nominal operation voltage of INTT is 100 V, to ensure full depletion.**)
- Two scintillators are located at the front and back of the INTT telescope, respectively. (Has coincidence)

  - Nominal size which has a size similar to that of the active area of the INTT half-ladder
- One fingertip scintillator with a size similar to that of the single cell of INTT sensor (optional)
- A camac module was introduced to measure the time duration between the previous trigger fired time and the time of the next Positron delivered (original idea, for detail please consult with Genki )
- The relative ladder positions in the beam direction were measured by a ruler: 0, 29.552 mm, 59.104 mm
- For the runs used in the analysis, the threshold setting is $\{15, 30, 60, 90, 120, 150, 180, 210\}$, unless otherwise specified.
- The readout system post ROC is different from that of used in 1008, BNL. In the beam test 2021, we were using the FEM system, while in the IR, 1008, the INTT data sent from ROCs are processed by FELIX board.

The links relevant to the beam test 2021 are listed below.

- Analysis code (Cheng-Wei's):
  - `https://github.com/ChengWeiShih/Final_BeamTest2021_Publication`.
- Everything including photos, data, and run log are in the the intt.sphenix@gmail.com
- The data log:
  - `https://docs.google.com/spreadsheets/d/1XZ7cTRjl9ra9Fn2CyHDyzguJkPW6anMDin0mukZS7D0/edit#gid=0`.
- The raw data on the Google drive:
  - `https://drive.google.com/drive/folders/1p8mPqi8WNISf8_FZ1YWar-f6DLSeKRde`.
- Beam test data log note:
  - `https://docs.google.com/document/d/1m-hrVRhi2o2VzA2zzFCdaDTRXIwtpWYWX2o0yOBav7I/edit#heading=h.t6qc45pquktu`.
- The data without the clone hit, based on Genki's criteria (link might be invalid):
  - `https://bnlbox.sdcc.bnl.gov/index.php/s/NkgitBnWSza3TeB`.

The runs used in the analysis are listed below.

- Run 52
  - Raw Data: **BeamData_20211210-0302_0.dat**.
  - One of the best runs taken during the beam test. Beam spot at the center of the ladder.
  - Run used for detection efficiency measurement, residual distribution comparison with MC, and potentially N reconstructed tracks compared with MC.
- Run 89
  - Raw Data: **BeamData_20211210-2043_0.dat**.
  - One of the best runs taken during the beam test. Beam spot touches the bottom edge of the ladder.
  - Run used for detection efficiency measurement.

- Run 61
  - Raw Data: **BeamData_20211210-0928_0.dat**.
  - Vertical rotation 13.7 degrees.
  - Run used for cluster phi size distribution study.
- Run 64
  - Raw Data: **BeamData_20211210-1125_0.dat**.
  - with Pb plate in between the beam and INTT telescope.
  - Run used for N reconstructed tracks compared with MC.
- Run 71 to 78
  - DAC Scan runs used for mapping the energy deposit distribution of the INTT sensor.
  - BeamData_20211210-1452_0.dat
  - BeamData_20211210-1501_0.dat
  - BeamData_20211210-1510_0.dat
  - BeamData_20211210-1519_0.dat
  - BeamData_20211210-1526_0.dat
  - BeamData_20211210-1534_0.dat
  - BeamData_20211210-1541_0.dat
  - BeamData_20211210-1549_0.dat

Common issues of beam test 2021 are listed below:

- The TDC module seems to be not working as expected
  - The TDC module is for measuring the time interval between the INTT BCO clock and external trigger timing. This is for the hypothesis to explain the 96% detection efficiency measured in the beam test 2019 in Fermilab (what we want is $> 99\%$). Since the beam itself was not synchronized with the INTT clock. It could possibly lead to low detection efficiency.
  - It's since a Windows PC was used for the final data storage, the order of the job processes can be varied according to how Windows manages the computing resources.
- In the event data, there is no trigger information
  - It may be due to the same reason as described above or simply too high rate. There are actually multiple events in one data event (maybe) associated with the trigger information of the first event.
  - But it's believed that all the events stored in the data have the trigger fired. It's just the trigger information not saved in the file, may be due to too high rate.
- The clone event
  - We found that sometimes there would be a group of hits that somehow could be identical to the adjacent group of hits. For example, groups A and B both have 3 hits, and the hits in group A have the same position and ADC information as that of group B.
  - Example is shown in Figure 2: From the data file of **BeamData_20211210-0302_0.root, Event 17, elements 48 to 55**.

- The identical group with bco_diff within 5 BCOs are discarded. (A new root file with the filename format of "**runXX_no_clone.root**" is produced by Genki, where XX is the run number.)

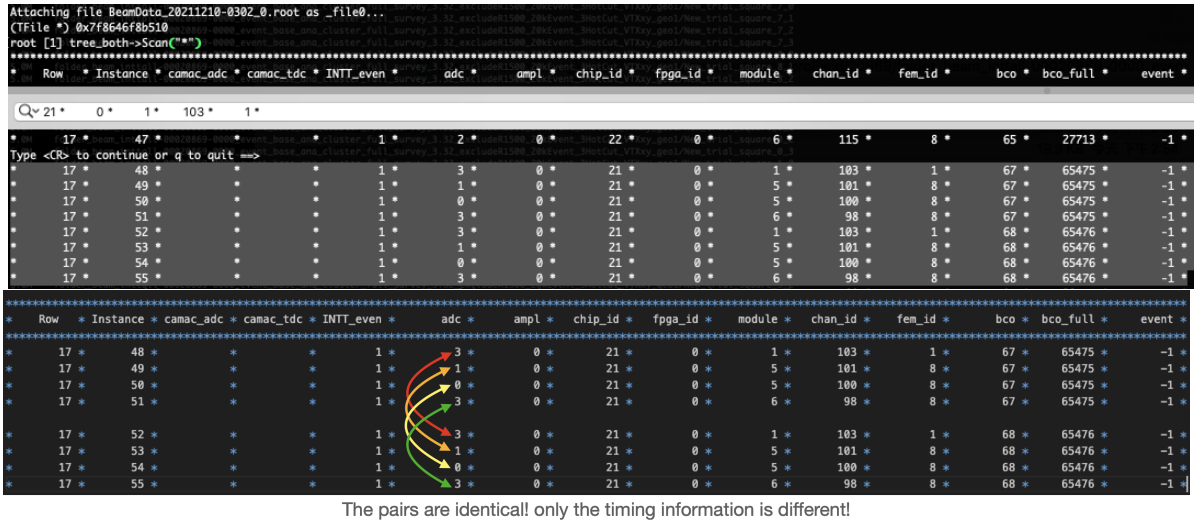


**Figure 2:** Top: raw hits printed by using ROOT. Bottom: the same raw hits but separated by bco_full. The colored arrows indicate the hits with identical positions and ADC information.

- The clone hits
  - With the same bco and bco_full, we don't expect to see two hits that have the same position information (module, chip_id, chan_id). The adc value can be different in this case.
  - The clone hits are removed from the analysis.

In the analysis, the tree of **tree_both** is used. The content of the **tree_both** is listed below.

- **adc**: hit adc, ranging from 0 to 7.
- **chip_id**: hit chip index, ranging from 1 to 26.
- **module**: basically the layer ID, 1 for layer0, 6 for layer1, and 5 for layer2.
- **chan_id**: hit channel index, ranging from 0 to 127.
- **bco_full**: global timing ranging from 0 - 65536 BCOs (one BCO = 106 ns)
- **bco**: hit local timing, ranging from 0 - 127 BCOs, incrementing together with bco_full.

The procedures before the major analyses are listed below:

- Decoding: from **.dat** files to **.root** files
- Clone event removal (by Genki's definition)
- Clone hit removal (by Cheng-Wei)
- Clustering (by Cheng-Wei)

– Hits are clustered using an adjacency graph. Two INTT hits are considered adjacent if and only if they share the same coordinate in $x$ and have touching edges in the $y$-axis direction. The cluster position in the $y$-axis is determined by the center-of-mass method. The weights of hits in one cluster are given by the converted hit adc. Ideally, these clusters represent the full extent of the energy deposition from a charged particle passing through an INTT layer and contain information about its location, timing, size, and energy. The example of clustering is shown in Figure 3.

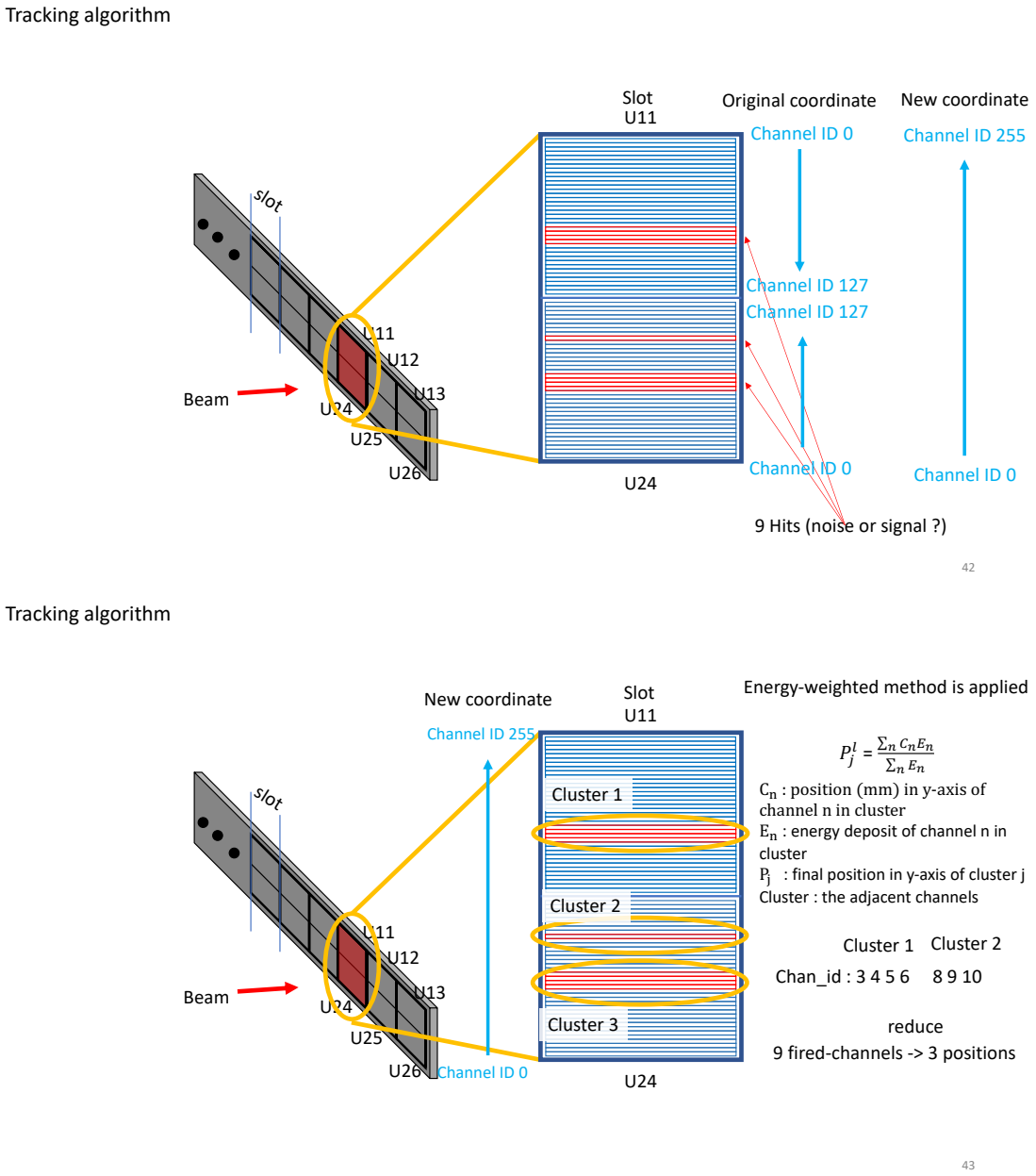


**Figure 3:** The example of clustering.

# 3 Energy Deposit distribution (DAC Scan)

The energy deposit distribution is mapped by performing the DAC Scan. The readout chip of INTT features a 3-bit adc (8 programmable converters), which limits the precision if one wishes to map the full energy deposition distribution in one shot. The DAC Scan was therefore performed via taking several runs with different threshold settings, as listed in Table 1. In each run, basically the last bin (8th bin) is the overflow bin, and is discarded. The ADC0 and ADC1 of a given run are identical to the adc5 and adc6 of its previous run, vice versa. By applying different weightings to match the two bins of distributions from different runs, the full energy deposit distribution with higher precision can be obtained.

| RunNumber | adc0 | adc1 | adc2 | adc3 | adc4 | adc5 | adc6 | adc7 |
|---|---|---|---|---|---|---|---|---|
| 71 | 88 | 92 | 96 | 100 | 104 | 108 | 112 | 116 |
| 72 | 108 | 112 | 116 | 120 | 124 | 128 | 132 | 136 |
| 73 | 128 | 132 | 136 | 140 | 144 | 148 | 152 | 156 |
| 74 | 148 | 152 | 156 | 160 | 164 | 168 | 172 | 176 |
| 75 | 8 | 12 | 16 | 20 | 24 | 28 | 32 | 36 |
| 76 | 28 | 32 | 36 | 40 | 44 | 48 | 52 | 56 |
| 77 | 48 | 52 | 56 | 60 | 64 | 68 | 72 | 76 |
| 78 | 68 | 72 | 76 | 80 | 84 | 88 | 92 | 96 |

**Table 1:** The threshold settings used for the DCA-scan runs.

Events with number of clusters in single layer greater than 1 [1], or with clone hits found are dropped. In addition, in the DAC Scan runs, the beam spot is at column 10, as shown in Figure 4. The columns other than 9, 10, 11 are discarded in the DAC Scan analysis. After the clustering, only single-hit clusters are filled into the histograms. In each histogram, the overflow bin (8th bin) is dropped. Figure 5 shows the raw hit adc distribution of each scan of each layer.

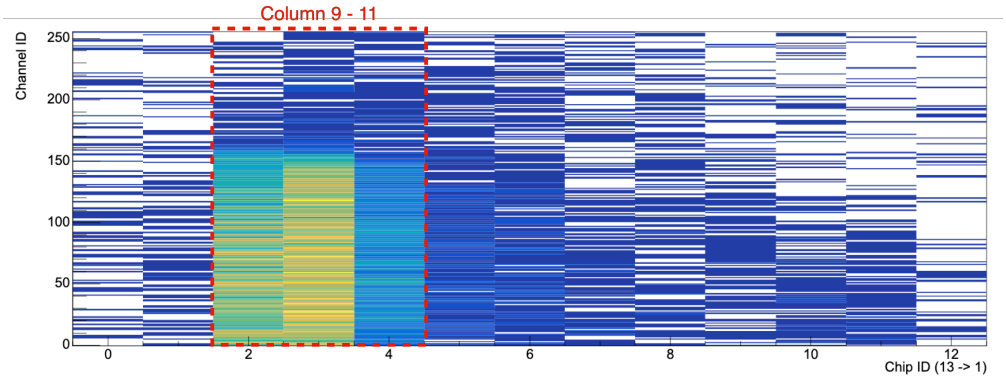


**Figure 4:** The hit map of a representative scan and layer.

[1] Requiring single cluster or no cluster in each layer (inclusive to location, and cluster size).

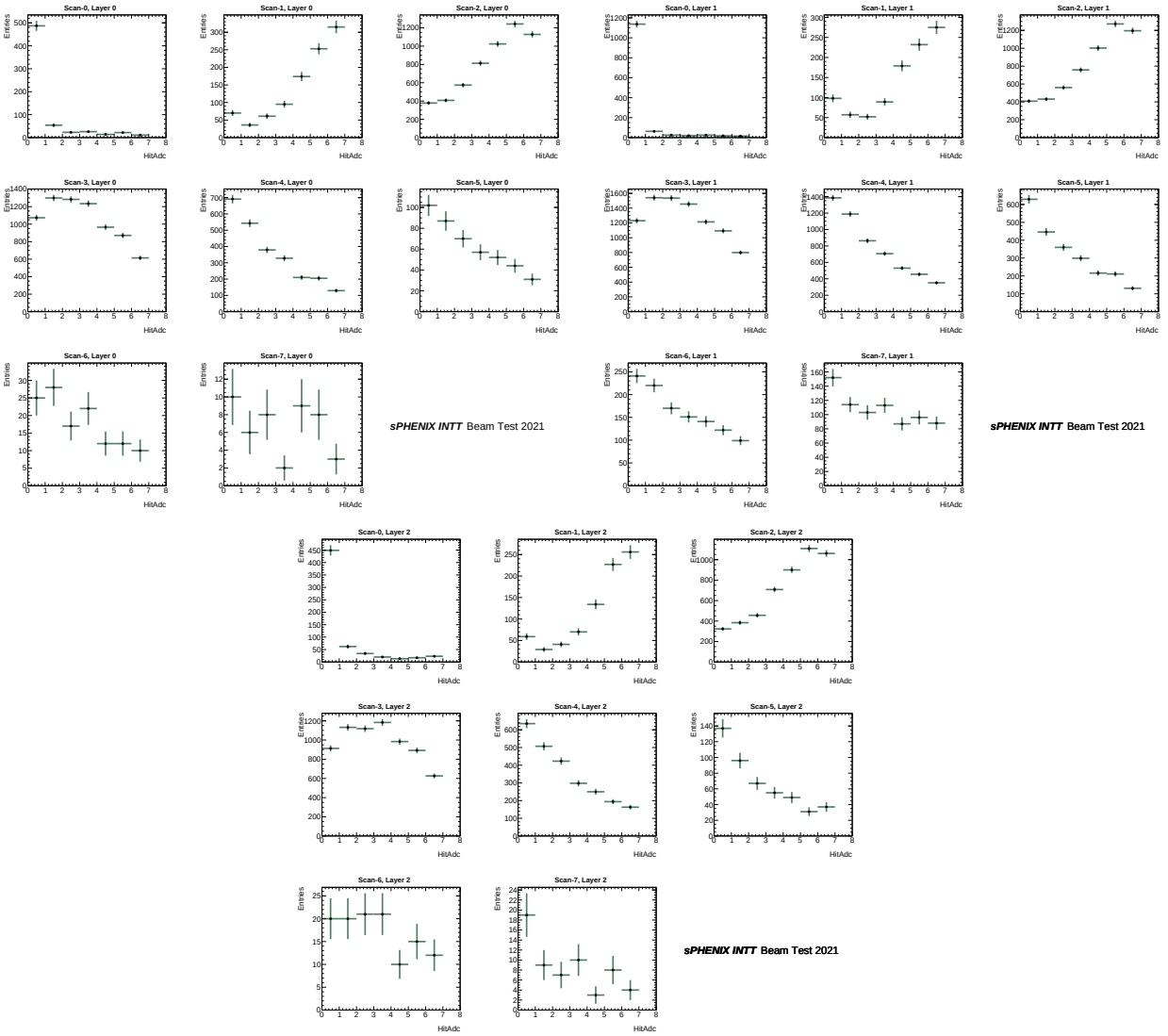


**Figure 5:** The raw hit adc distribution of each scan. Only the single-hit clusters are filled. Layer-0, Layer-1, and Layer-2 are presented from the top to bottom. In this section, the plots are presented following the convention, top-left: layer-0, top-right: layer-1, and bottom: layer-2.

As mentioned, there are two bins overlapped with its next scan, which are used for matching distributions. The Scan3 (Run 78), which covers the Most Probable Value (MPV), is used as the reference. The scale factors are introduced to the adjacent scans to sequentially match the distributions [2]. Taking the Scan4 (Run 71) as an example, the scale factor applied to the distribution of Scan4, $SF_{Scan4}$, is given in Equation 1. Figure 6 shows the ADC distributions of all scan runs after the scaling in three layers. A falling-shaped background component followed by the signal component can be observed.

[2]By sequential, what it means is Scan2 been scaled based on Scan3. And then Scan1 been scaled based on Scan2, and so on.

$$SF_{Scan4} = \frac{Size^{Scan3}_{bin_6} + Size^{Scan3}_{bin_7}}{Size^{Scan4}_{bin_0} + Size^{Scan4}_{bin_1}} \tag{1}$$

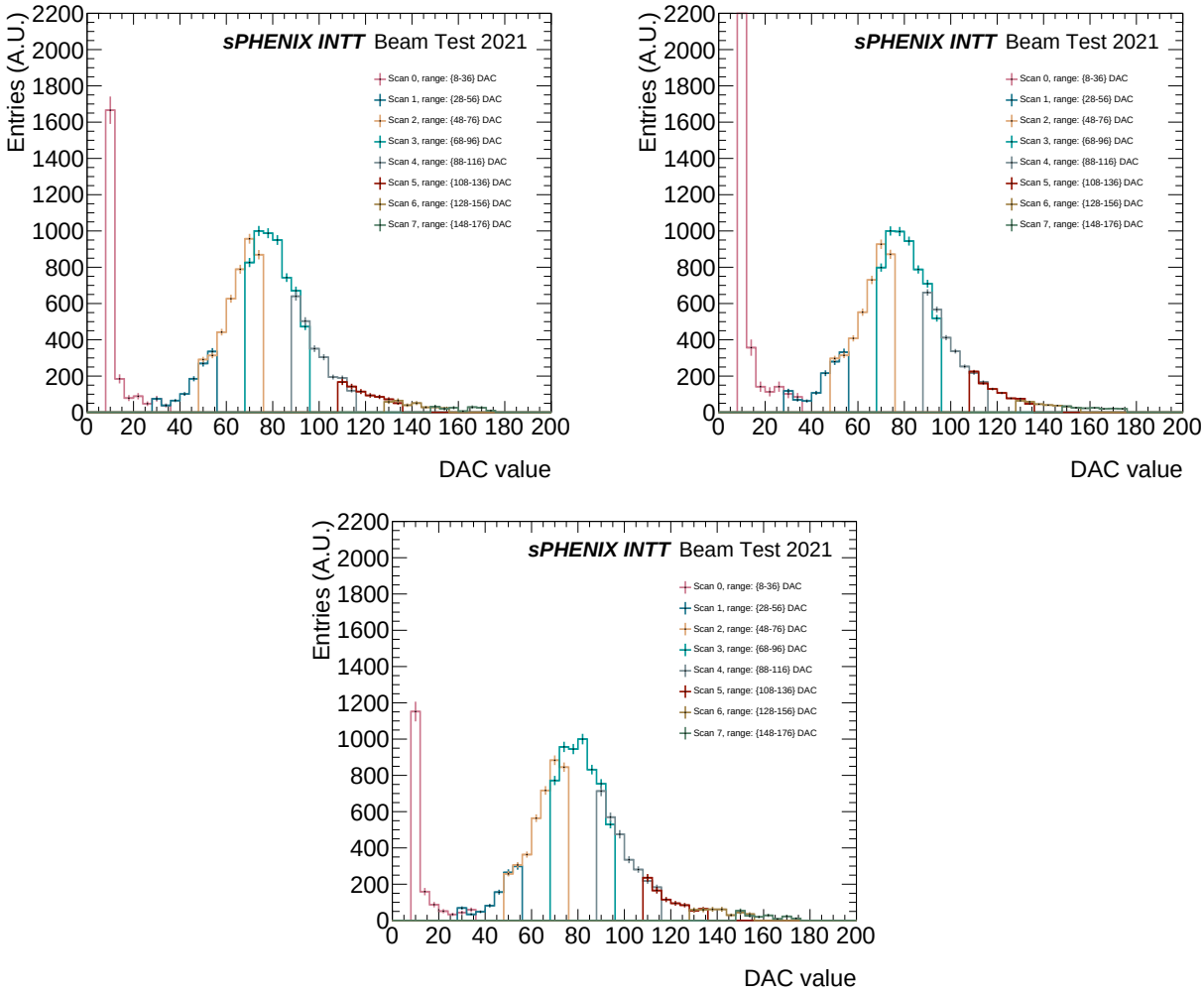


**Figure 6:** The ADC distributions of the eight scans after scaling. The legend indicates the scanning region of the scans.

In each layer, the overlapped bins are statistically combined. The weighted average of the two overlapped bins, $\bar{X}$, and the uncertainty of the weighted average result, $\sigma_X$, are calculated as:

$$\begin{aligned} \bar{X} &= \frac{A \cdot w_A + B \cdot w_B}{w_A + w_B}, \\ \sigma_X &= \begin{cases} \sqrt{\frac{1}{w_A + w_B}}, & if\ \chi^2/NDF \leq 1 \\ \sqrt{\frac{1}{w_A + w_B}} \cdot \sqrt{\chi^2/NDF}, & \text{otherwise,} \end{cases} \end{aligned} \tag{2}$$

where $A$ and $B$ are the bin contents of the overlapped bins, respectively, and $w_A$ and $w_B$ are computed as $1/[(stat.\ errors\ of\ the\ bins)^2]$. If the Reduced $\chi^2$ is greater than 1, the corresponding error, $\sigma_X$ is inflated by $\sqrt{\chi^2/NDF}$. The method is introduced by PDG [1]. The method is used mainly to account for the discrepancies observed in the overlap bins between Scan2 and Scan3. The energy deposit distributions of three layers after combination are shown in Figure 7. The distributions are fit with a function with a Landau-Gaussian convolution function for the signal component, and Exponential and Gaussian functions [3] for the background component [4]. For the region of ADC $\geq$ 40, the signal purity can be better than 99.3% for all three layers.

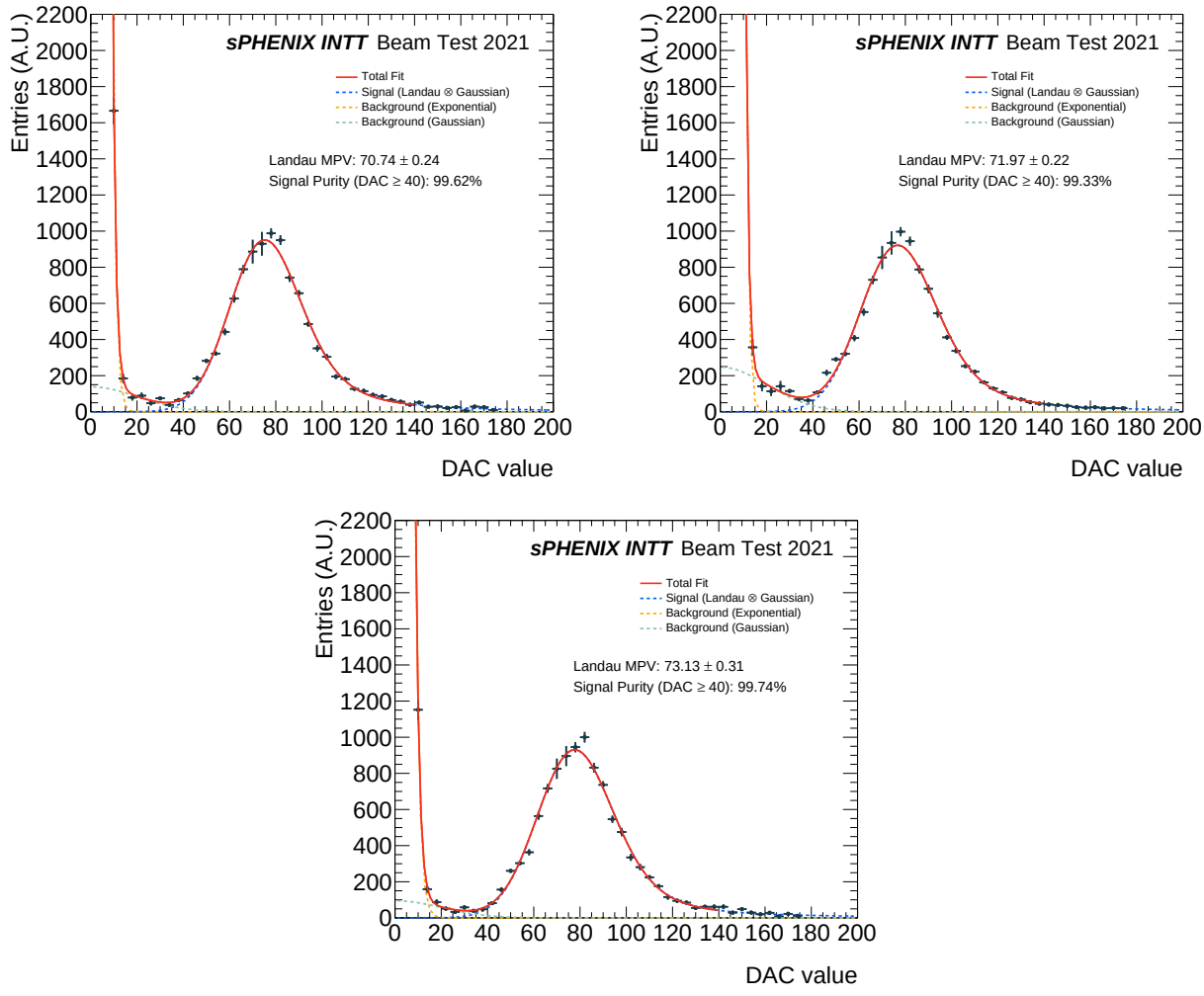


**Figure 7:** Energy deposit distributions of INTT of the three layers.

[3]For the Gaussian component, the limit of width is set to be 20, and the mean value is fixed at 0.
[4]The fit range is from 8 to 140 ADC

## 3.1 Final, including systematic uncertainty

In Figure 6, one can find that in the Scan2 and Scan3, the tendencies of overlapped bins do not agree each other [5]. The tendencies should in principle agree since those bins have identical energy deposit coverage. The reason of the disagreement remains unknown, but it does not change the message we want to deliver [6]. And thank you Akitomo who pointed out that since the matching is performed sequentially, the scales of distributions of Scano to Scan2 can be affected if the matching between Scan2 and Scan3 has any potential issues. We therefore examine the method used to match Scan2 and Scan3. The 7th bin of Scan2 is dropped, and only the 6th bin of Scan2 and 1st bin of Scan3 are considered in computing the scaling factor for the distribution of Scan2 as the variation, as shown in Figure 8.

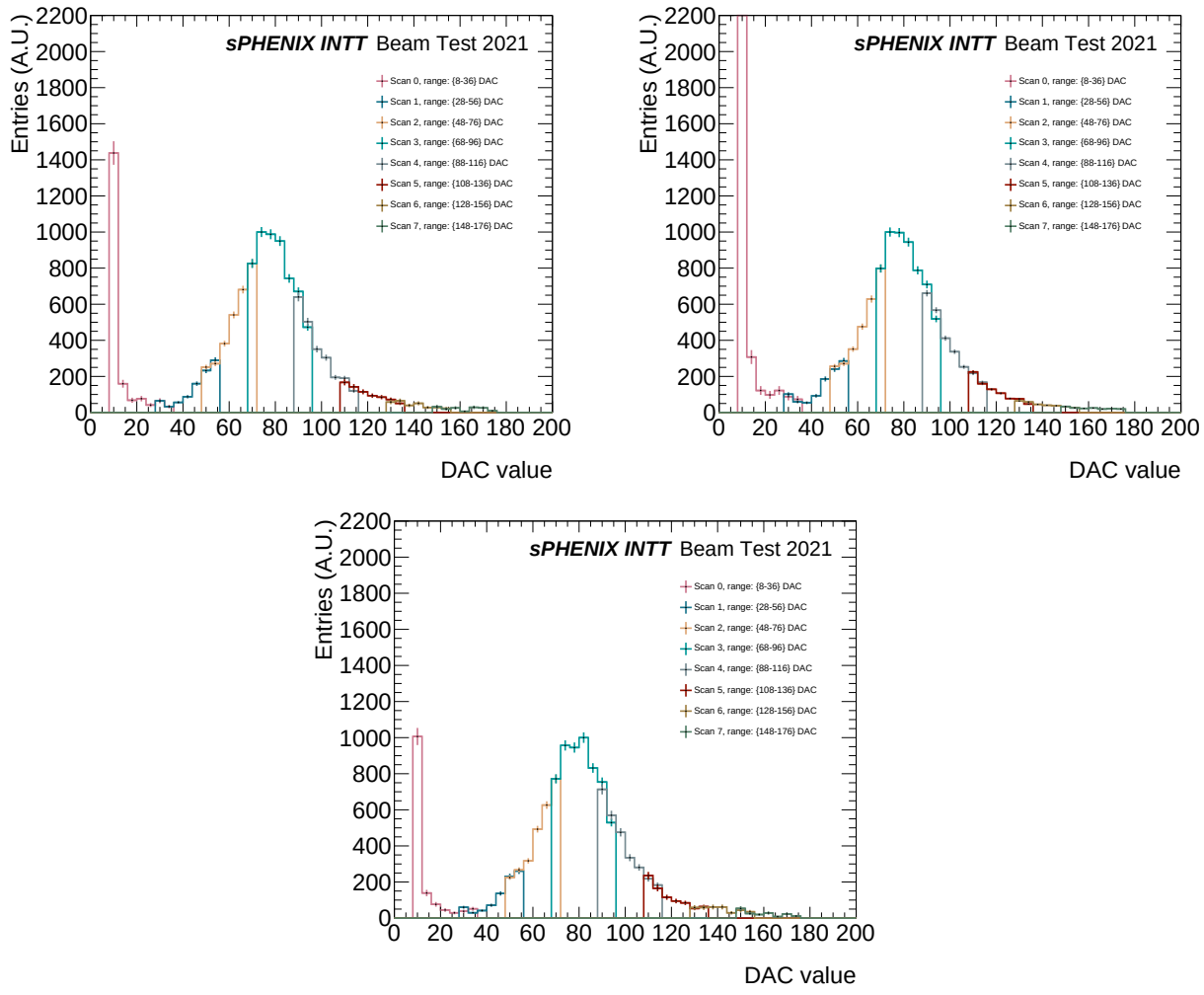


**Figure 8:** The ADC distributions of the eight scans after scaling. The difference comparing to Figure 6 is that in calculating the scaling factor for Scan2 distribution, only the 6th bin of Scan2 and 1st bin of Scan3 are considered.

[5] In Scan2, the slope of 6th and 7th bins is negative, while in Scan3, the slope of 1st and 2nd bins is positive.
[6] The evident signal spectrum, and high signal purity.

Figure 9 shows the energy deposit distributions with different approaches to match Scan2 and Scan3 distributions. The differences are quoted as the systematic uncertainty, as shown in Figure 10.

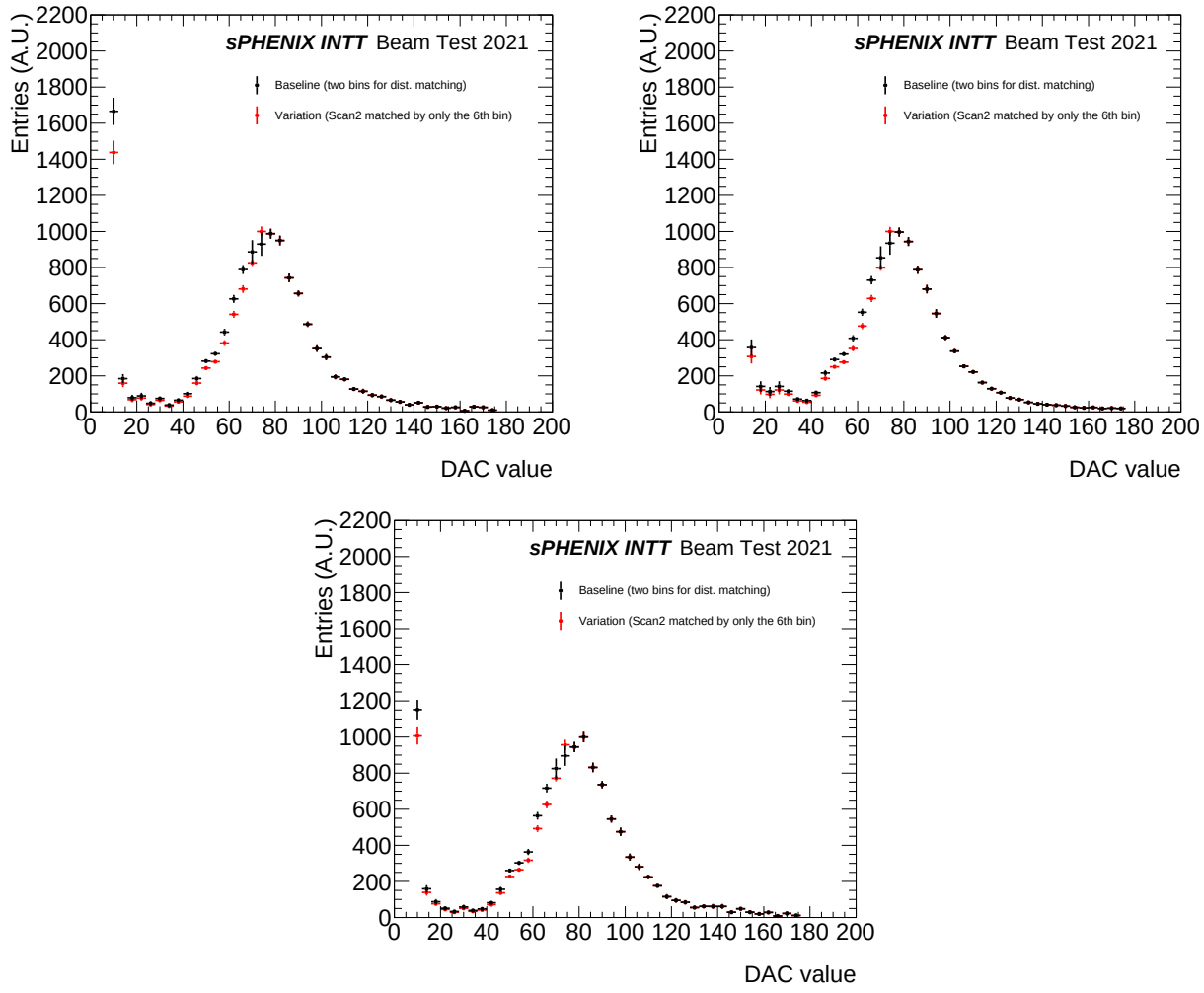


**Figure 9:** Energy deposit distributions with different approaches to match Scan2 and Scan3 distributions. The black circles are from Figure 7, which are using nominal combination method.

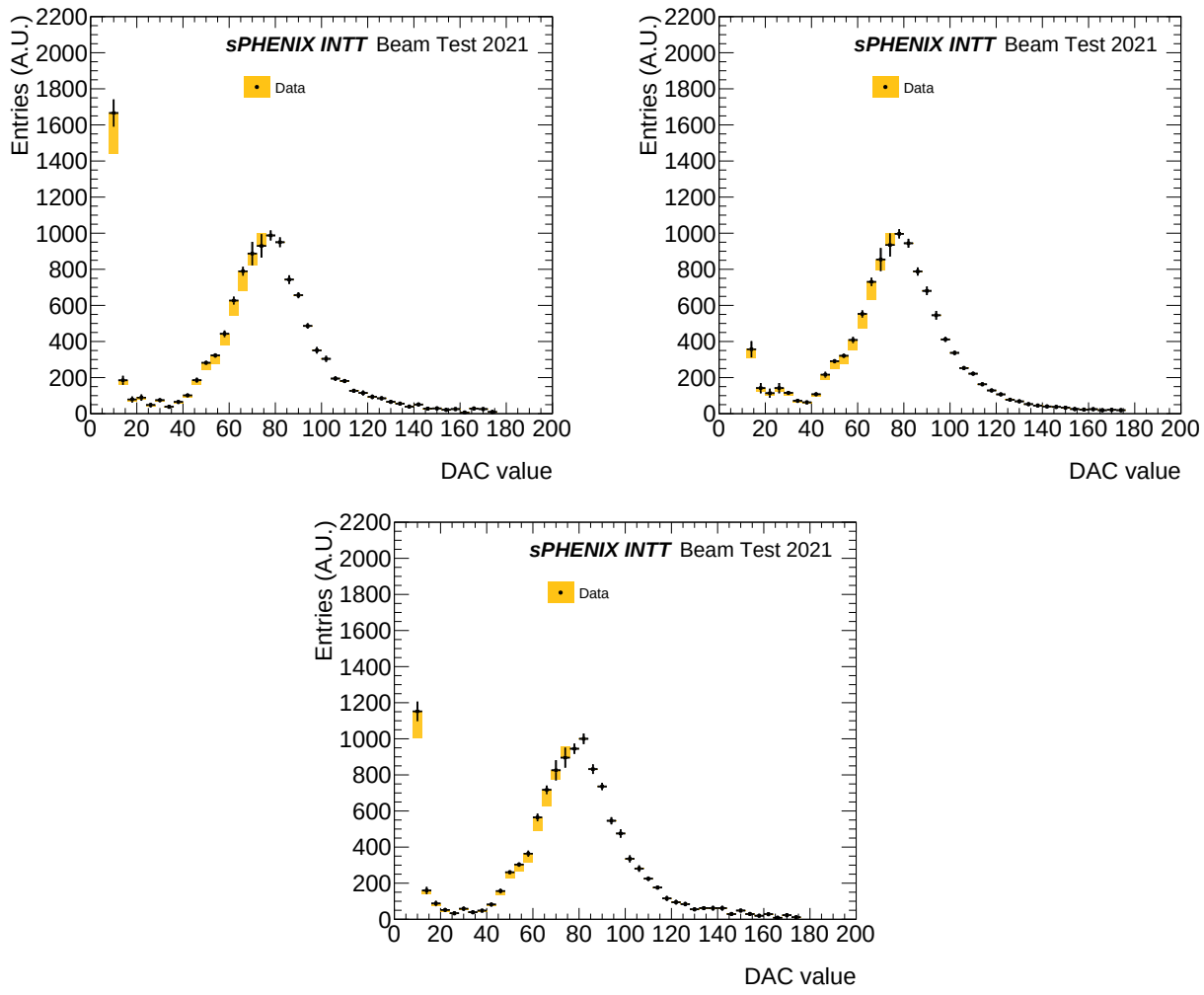


**Figure 10:** Energy deposit distributions of INTT of the three layers. The black vertical lines are the statistical uncertainties, and the yellow boxes represent the systematic uncertainties due to different ways of matching distributions in Scan2 and Scan3.

In each bin, the statistical and systematic uncertainties are summed in quadrature. The same fitting procedure is performed, as shown in Figure 11. The main message does not change. For the region of ADC $\geq$ 40, the signal purity can be better than 99.3% for all three layers.

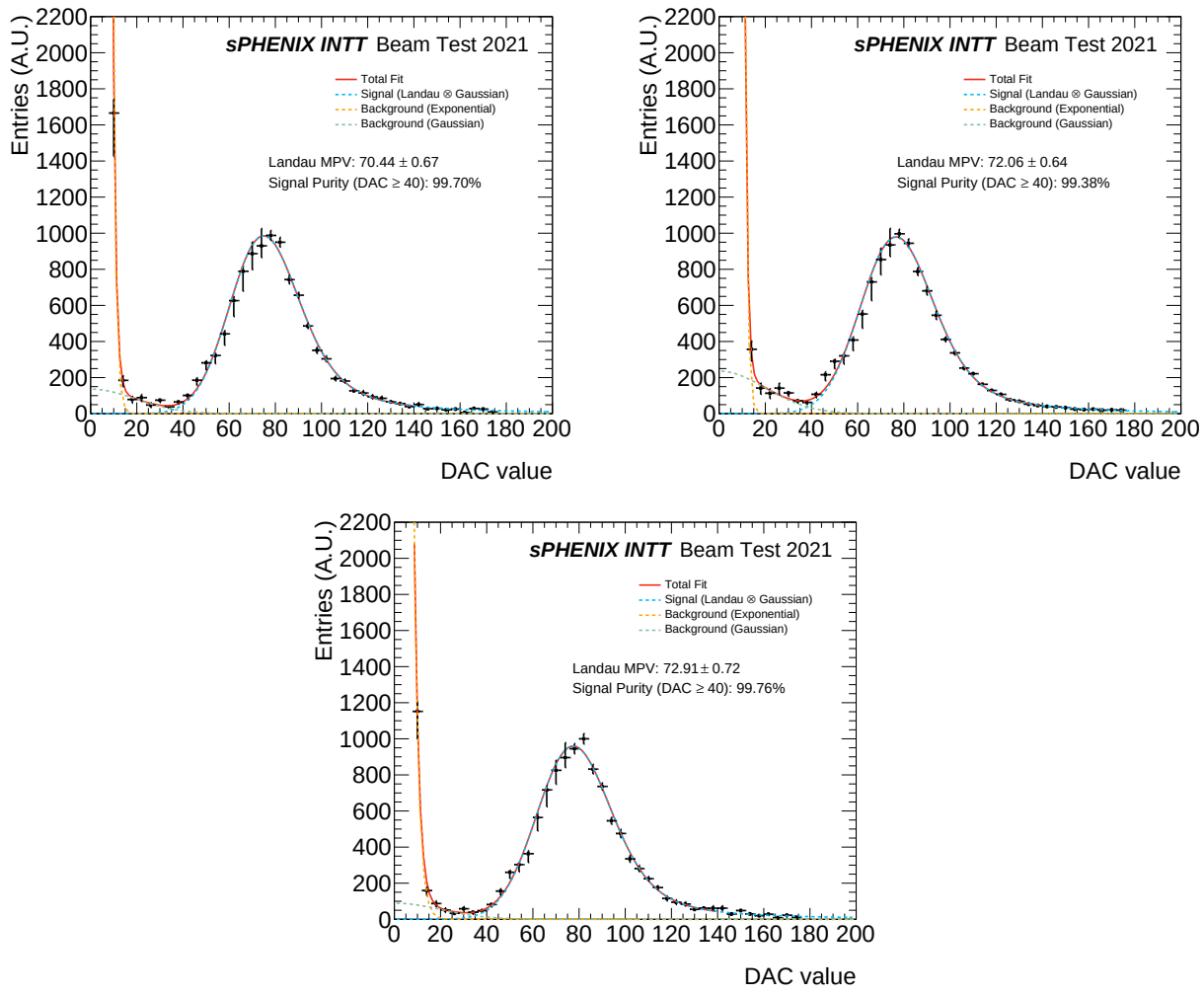


**Figure 11:** Energy deposit distributions of INTT of the three layers. The black vertical lines represent the total uncertainties, where the statistical and systematic uncertainties are summed in quadrature. Recap, in this section, the plots are presented following the convention, top-left: layer-0, top-right: layer-1, and bottom: layer-2.

# 4 Residual distribution compared with MC

In this topic, data Run52 is used. And we focus on column U8, which is within the beam spot region. The method used is to first reconstruct the proto-track by ladder L0 and L1. When good proto-track is found, we then check clusters in L2. The same procedures are performed with both data and MC. Before the event selection, the L1 alignment correction and proto-track slope re-centering [7] is applied. Figure 12 shows the L1 cluster residual distributions (L1 cluster - position obtained by L0L2 interpolation) before and after the correction. Figure 13 shows the proto-track slope distribution, before and after the re-centering.

[7]The re-centering is not a correction. It just moves the distribution to make it peak close to zero, for applying a symmetric slope cut afterwards.

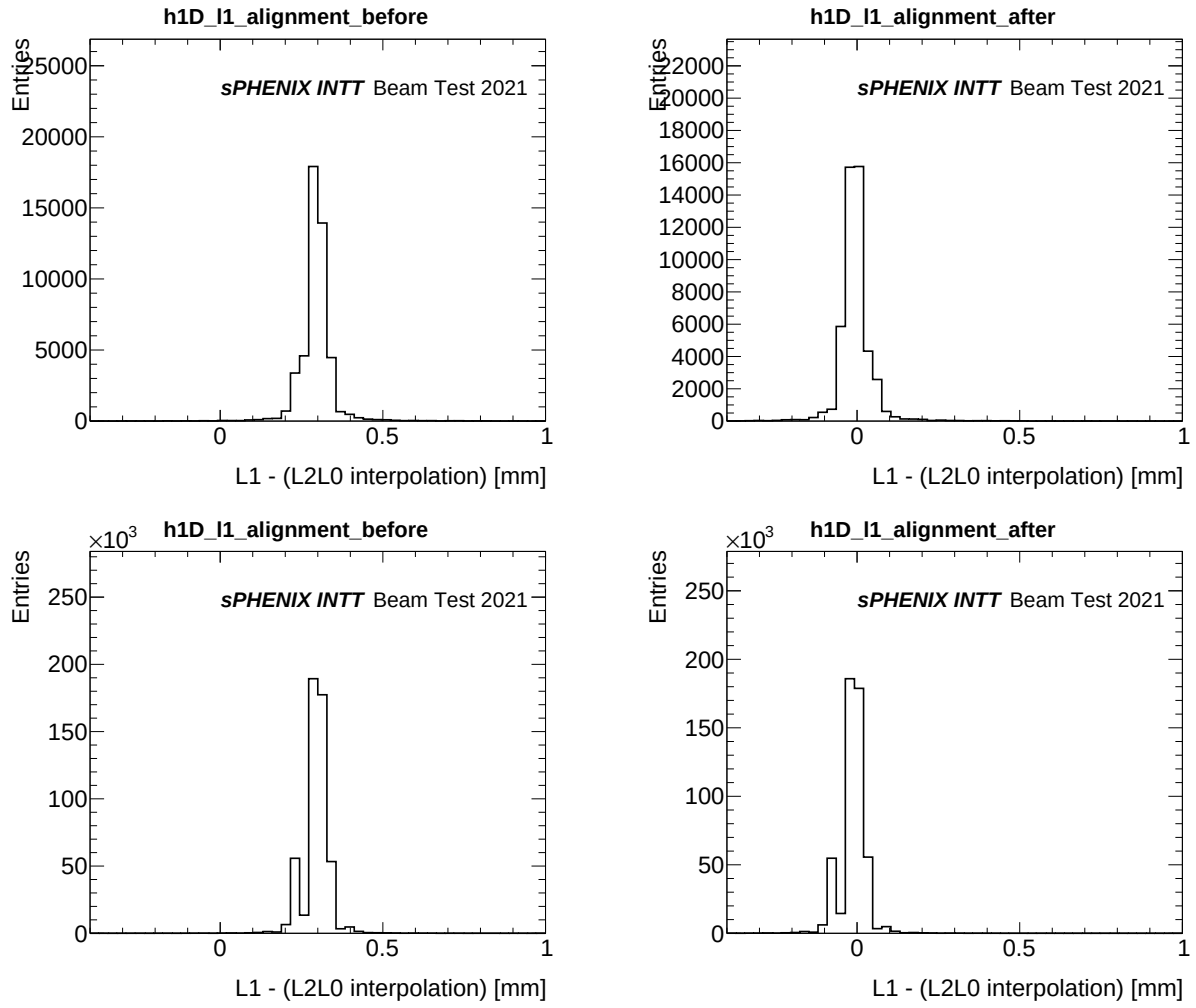


**Figure 12:** Residual distribution of L1 clusters before (left) and after (right) applying correction for data (top) and MC (bottom).

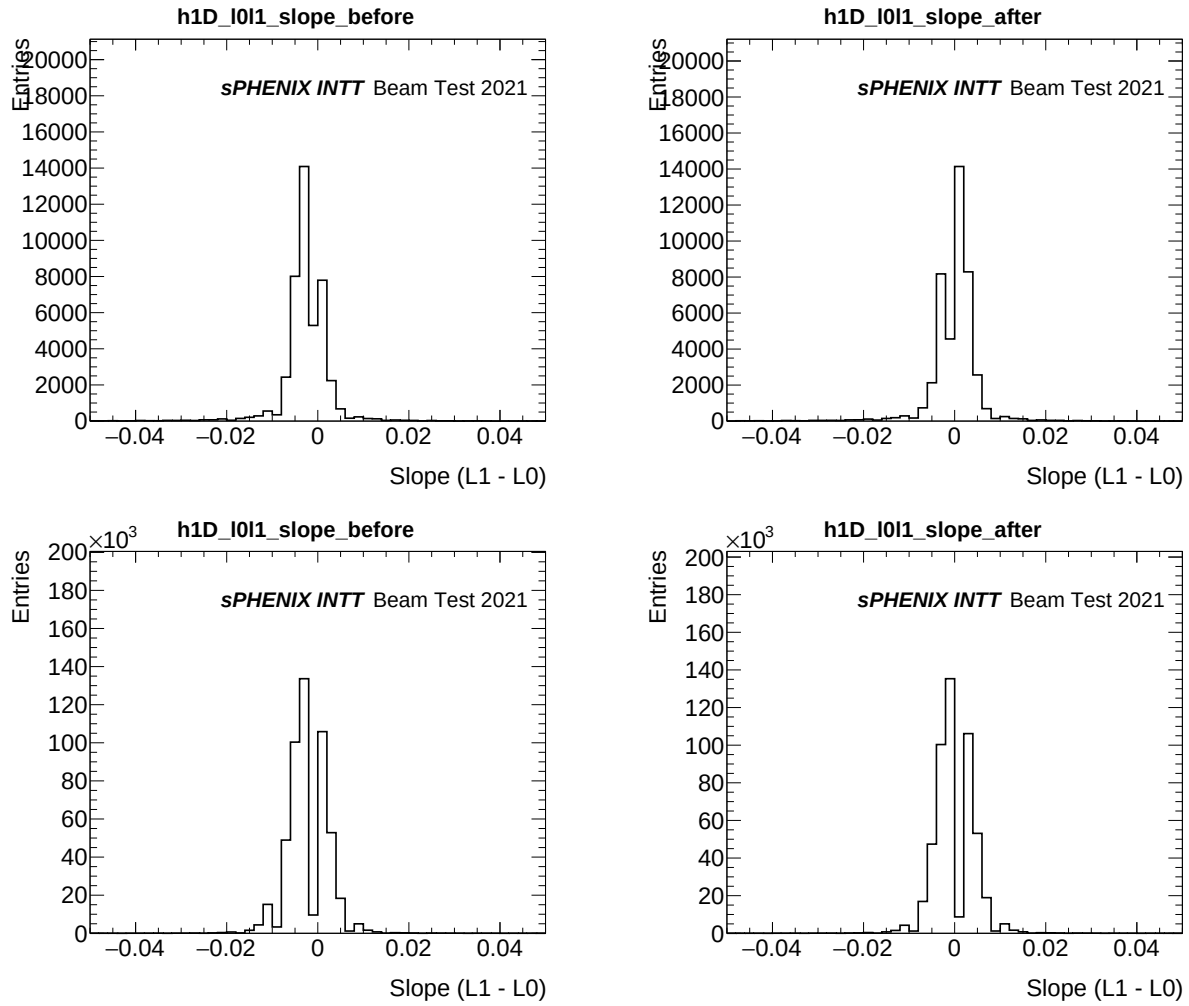


**Figure 13:** Proto-track slope distribution before (left) and after (right) applying re-centering for data (top) and MC (bottom).

For both data and MC, the event selections are described below.

- Events with clone hits are removed.
- Single cluster in each layer is required.
- The single cluster has to be at the Selected Column (SC).
- The slope of the proto-track is required to be within $\pm 0.01$.
- The position of the proto-track is required to be within $\pm 5$ mm in Y axis. Note that the ladder coverage in Y axis is $\pm 10$ mm. This selection controls the proto-track distribution, to allow clusters in L2 to have sufficient space for scattering.

For events pass the selections, the residual of L1 cluster is filled into histogram, where the residual of L1 cluster is calculated by **L1 cluster position - the position obtained by clusters L2&L0 interpolation.** The result is shown in Figure 14. The agreement between data and MC is reasonable well.

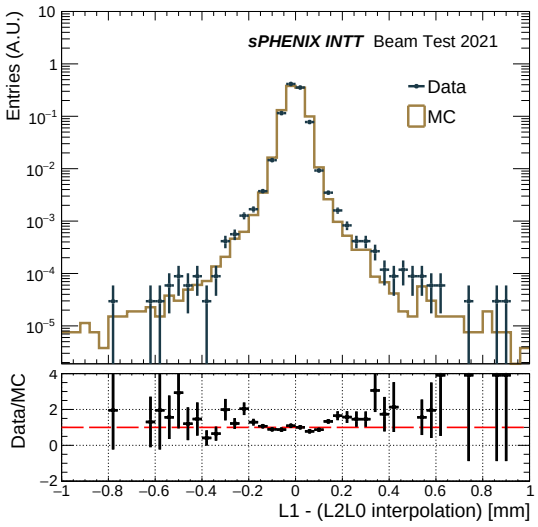


**Figure 14:** Distributions of L1 cluster residual from both data and MC, where the L1 cluster residual is obtained by **L1 cluster position - the position obtained by interpolation of clusters in L2 and L0.**

# 5 Ladder hit detection efficiency

The hit detection efficiency is the main topic of this beam test. The method of Detector Under Test (DUT) is used to evaluate the hit detection efficiency of INTT ladder. The DUT method requires a system to reconstruct tracks, and a detector to be tested (DUT layer) in middle of the system. By doing so, when a good (straight) track is reconstructed, we are then sure that this track should have passed through the DUT layer as well. We then check the clusters of the DUT layer. In the INTT beam test 2021, three INTT ladders are working functionally, and unlike the beam test facility of CERN, there is no additional system available for track reconstruction. Therefore, the INTT ladders L0 and L2 are used for track reconstruction, and the ladder L1 is the DUT layer. As mentioned, the track is first reconstructed by L0 and L2. When a good (straight) track is found in one event, the clusters in L1 is then checked.

In this analysis, Run52 and Run89 are used. Before the event selection, the L1 alignment correction and L0L2 slope re-centering [8] are applied. The event selections are listed below.

- Events with clone hits found are discarded.
- Single cluster in Selected Column (SC) of L0 (abbr.: SCL0) and L2 (abbr.: SCL2) required.
  - This is to minimize the ambiguity of track reconstruction (Only two layers for track reconstruction, to improve the purity, tight selection required)
- For three layers, require no cluster in adjacent columns (SC-1 & SC+1).
  - This is to account for the misalignment in the longitudinal axis (x axis).
- **Edge exclusion:** (ladder bottom edge + 8 ch) $<$ Y-pos of SCL0 and SCL2 $<$ (ladder top edge - 8 ch).

[8] Again, the re-centering is for applying a symmetric slope cut.

- This is to account for the misalignment in the transverse axis (y axis).

- **Cluster ADC:** Cluster Adc of SCL0 $>$ adco && Cluster Adc of SCL2 $>$ adco.
  - This is to minimize tracks reconstructed by noise hits (Only two layers for track reconstruction, to improve the purity, tight selection required.)
- **Slope cut:** $|$slope of SCL2 - SCL0$| < 0.01$.
  - This is to make sure that reco. tracks are coming from the beam. The distribution of slope of SCL2 and SCL1 is shown in Figure 15.

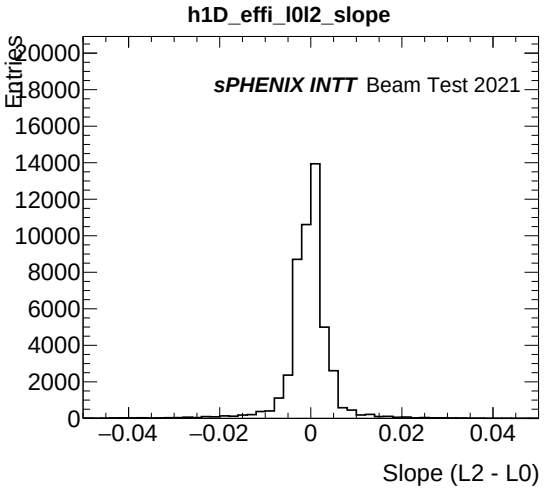


**Figure 15:** The distribution of slope of SCL2 and SCL1 of Run52 U8.

- **Track Position:** Focus on beam spot region (Run52: -6 to 6 mm, Run89: -10 to 2 mm)
  - This is to make sure that reco. tracks are coming from the beam. The beam spot region is monitored by the distribution of cluster position, as shown in Figure 16.

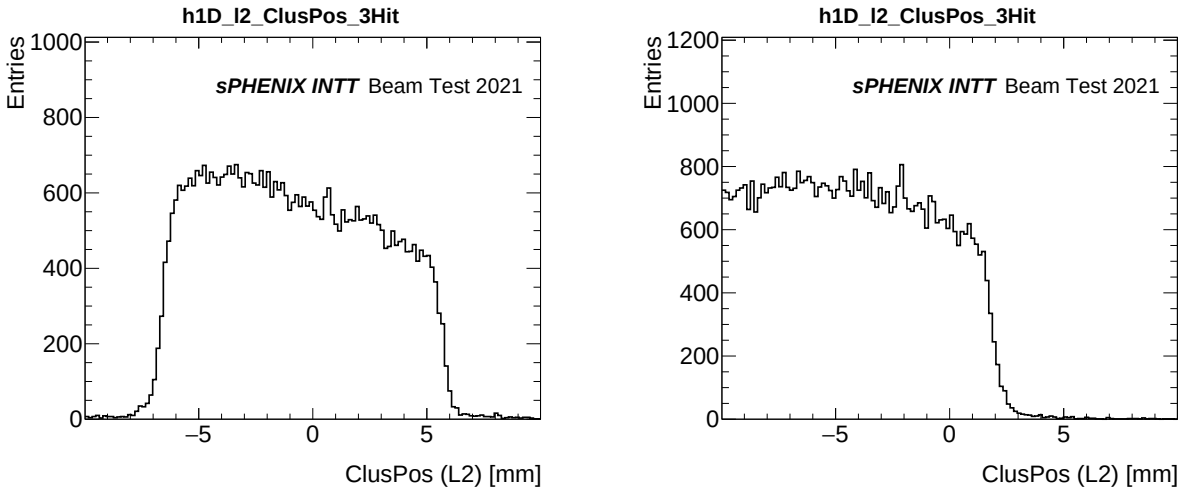


**Figure 16:** Distribution of cluster position in Y axis for Run52 U8 (left) and Run89 U10 (right), respectively.

Events that pass the selections mentioned above are then considered as good events. Clusters in L1 of the event are then checked. If there is no cluster found in SCL1 or the smallest residual [9] is greater than 0.5 mm, the L1 is then classified as failed to detect the particle hit in this event. The detection efficiency is defined in Equation 3.

$$Effi. = \frac{\text{Good Events and L1 Good Cluster Found}}{\text{Good Events}} = \frac{N(L0 \bigcap L1 \bigcap L2)}{N(L0 \bigcap L2)}, \tag{3}$$

where the $N(L0 \bigcap L2)$ is the number of events with good tracks formed by clusters in L0 and L2, and $N(L0 \bigcap L1 \bigcap L2)$ is the number of events with L1 clusters that can match to the reconstructed L0-L2 track well. Table 2 shows the measured INTT ladder hit detection efficiency for Run52 and Run89. In addition, the systematic uncertainties affecting the detection efficiency measurement are evaluated, as also shown in the table. The considered sources are the column dependency, Residual cut, slope cut, and the boundary cut. The amount of the variation is shown in Table 2 as well. The results with tested variations all give efficiencies above 99%.

| Source | Variation | Run52 | | | Run89 | | |
|---|---|---|---|---|---|---|---|
| | | Numerator | Denominator | Efficiency(%) | Numerator | Denominator | Efficiency(%) |
| **Baseline** | | 42956 | 43099 | **99.668** | 50491 | 50746 | **99.497** |
| Column | U8 → U9 (Run52)<br>U10 → U11(Run89) | 44198 | 44301 | **99.768** | 37148 | 37338 | **99.491** |
| Residual Cut | 0.5 mm → 0.7 mm | 42972 | 43099 | **99.705** | 50511 | 50746 | **99.537** |
| | 0.5 mm → 0.3 mm | 42895 | 43099 | **99.527** | 50436 | 50746 | **99.389** |
| Slope Cut | 0.01 → 0.013 | 43638 | 43795 | **99.642** | 51359 | 51623 | **99.489** |
| | 0.01 → 0.007 | 41748 | 41877 | **99.692** | 48622 | 48856 | **99.521** |
| Boundary Cut | 8 ch → 11 ch | 42956 | 43099 | **99.668** | 49378 | 49625 | **99.502** |
| | 8 ch → 5 ch | 42956 | 43099 | **99.668** | 51609 | 51873 | **99.491** |

**Table 2:** Table of the measured INTT ladder hit detection efficiency for Run52 and Run89, with different variations considered for systematic uncertainty estimation.

The hit detection efficiency as a function of Y axis is also measured. Figure 17, 18, 19, and 20 show the hit detection efficiency as a function of Y axis compared to the same distributions but with variations in column, residual cuts, slope cuts, and boundary cuts, respectively.

[9] Residual: cluster in L1 - LoL2 interpolation.

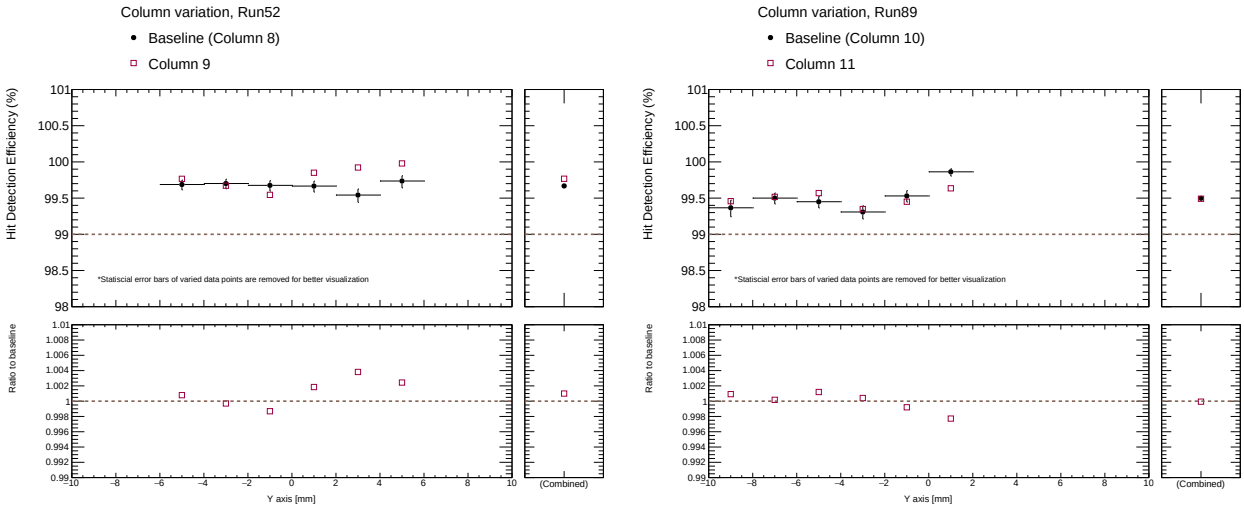


**Figure 17:** Ladder hit detection efficiency for different columns for Run52 (left) and Run89 (right). The right panel shows the result inclusive to the track position.

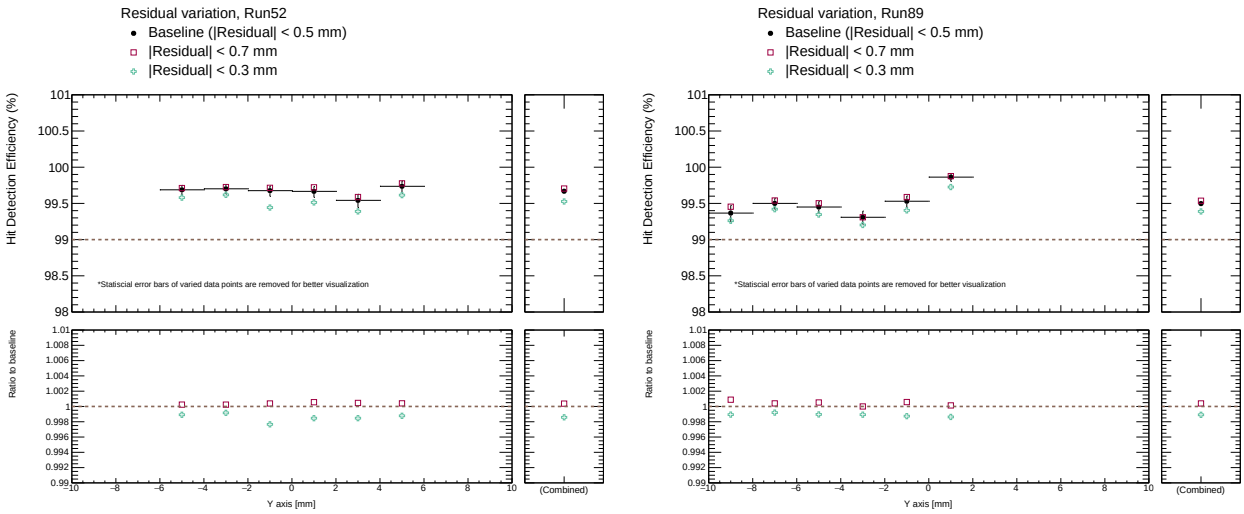


**Figure 18:** Ladder hit detection efficiency for different residual cuts for Run52 (left) and Run89 (right). The right panel shows the result inclusive to the track position.

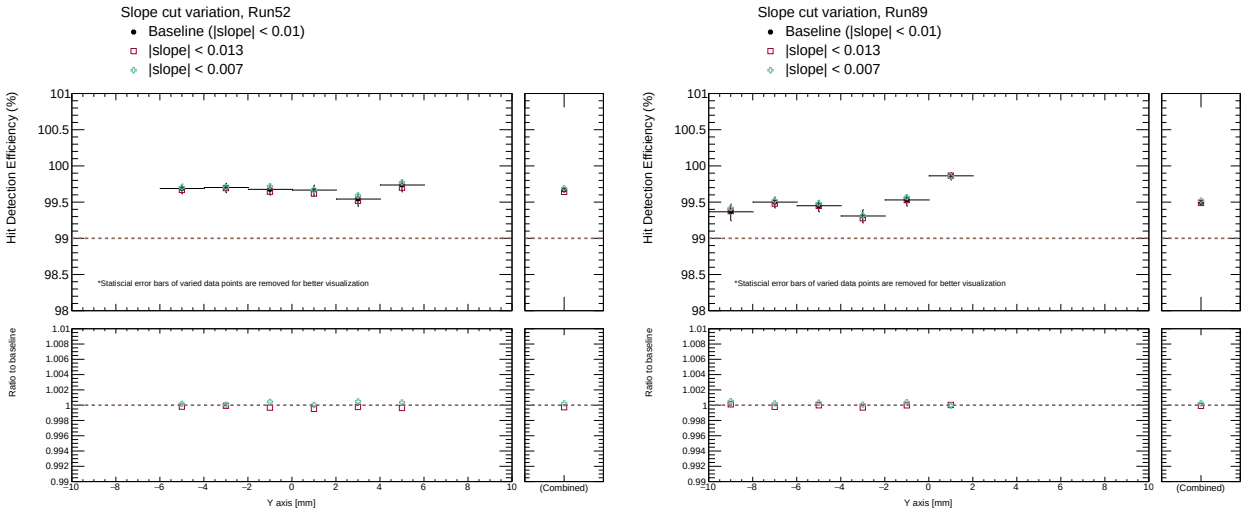


**Figure 19:** Ladder hit detection efficiency for different slope cuts for Run52 (left) and Run89 (right). The right panel shows the result inclusive to the track position.

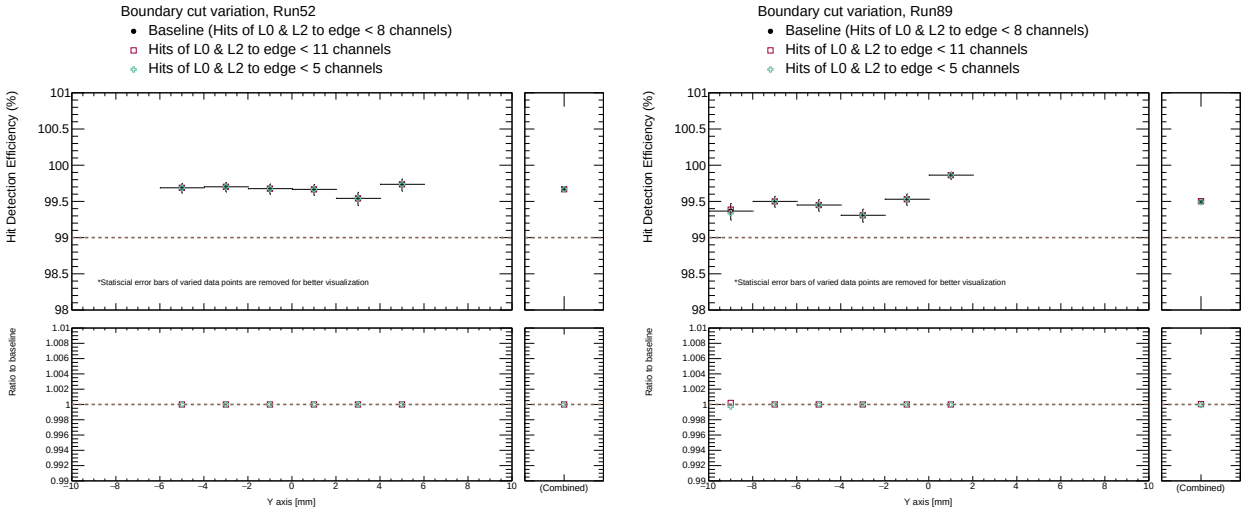


**Figure 20:** Ladder hit detection efficiency for different boundary cuts for Run52 (left) and Run89 (right). The right panel shows the result inclusive to the track position.

The total systematic uncertainty in each bin is obtained by summing all sources in quadrature under the assumption that individual uncertainties are independent and uncorrelated, as shown in Figure 21. The largest uncertainty is the column dependency and the residual cut variation.

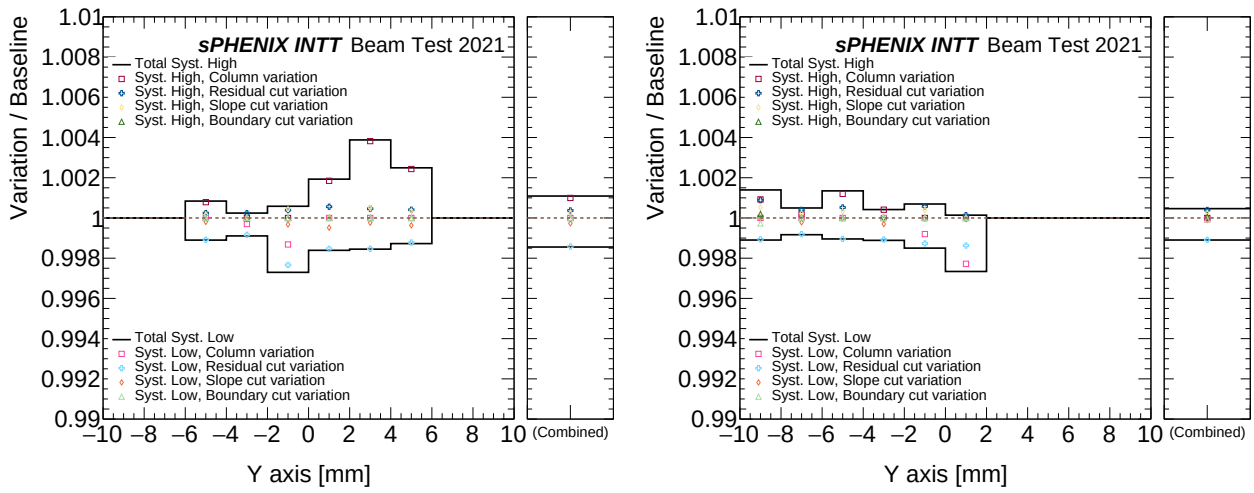


**Figure 21:** Total systematic uncertainty as a function of Y axis (the track position) for Run52 (left) and Run89 (right). The right panel shows the result inclusive to the track position.

The final measured INTT ladder hit detection efficiency is shown in Figure 22 for Run52 and Run89. In terms of numbers, they are listed in Equation 4.

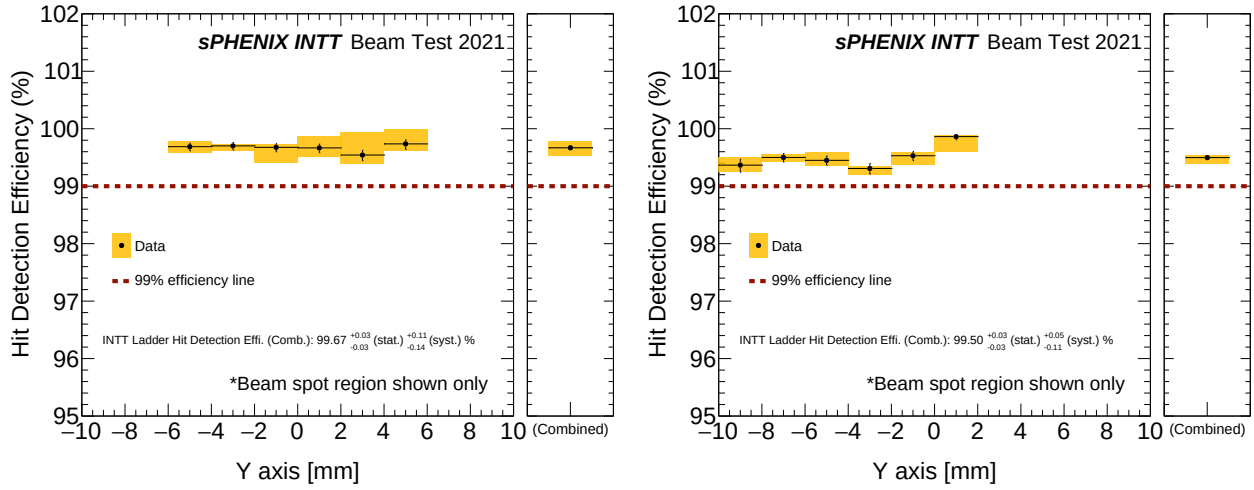


**Figure 22:** The final measured INTT ladder hit detection efficiency as a function of Y axis for Run52 (left) and Run89 (right). The right panel shows the result inclusive to the track position. The vertical extent of each box represents the total systematic uncertainty, while the vertical line shows the statistical uncertainty.

$$
\begin{aligned}
Run52 &= 99.668\ ^{+0.028}_{-0.030}(stat.)\ ^{+0.109}_{-0.144}(syst.)\% \\
Run89 &= 99.497\ ^{+0.031}_{-0.033}(stat.)\ ^{+0.046}_{-0.109}(syst.)\%
\end{aligned}
\tag{4}
$$

To have better coverage in the Y axis, and to increase the statistics, the Run52 and Run89 are combined, as shown in Figure 23, 24, 25, and 26.

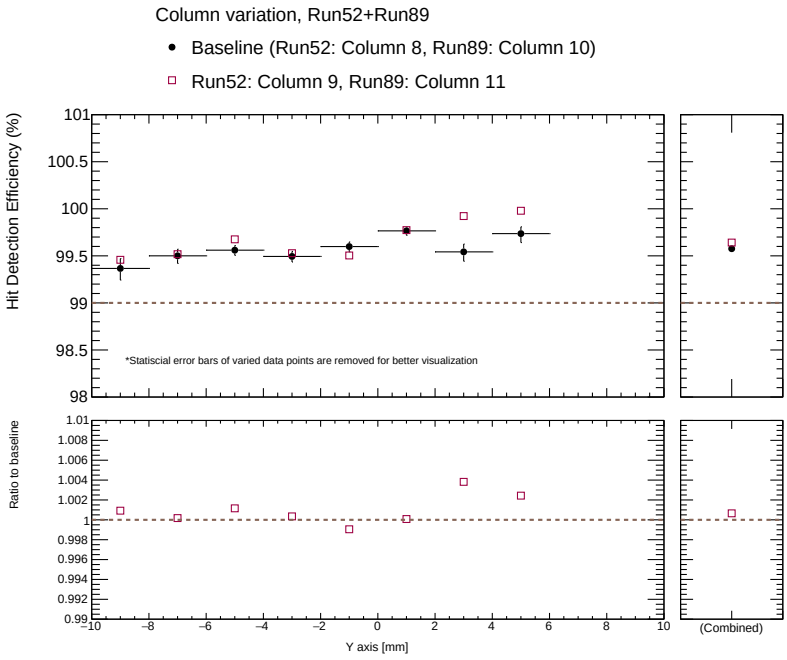


**Figure 23:** Ladder hit detection efficiency for different columns for Run52 and Run89 combined. The right panel shows the result inclusive to the track position.

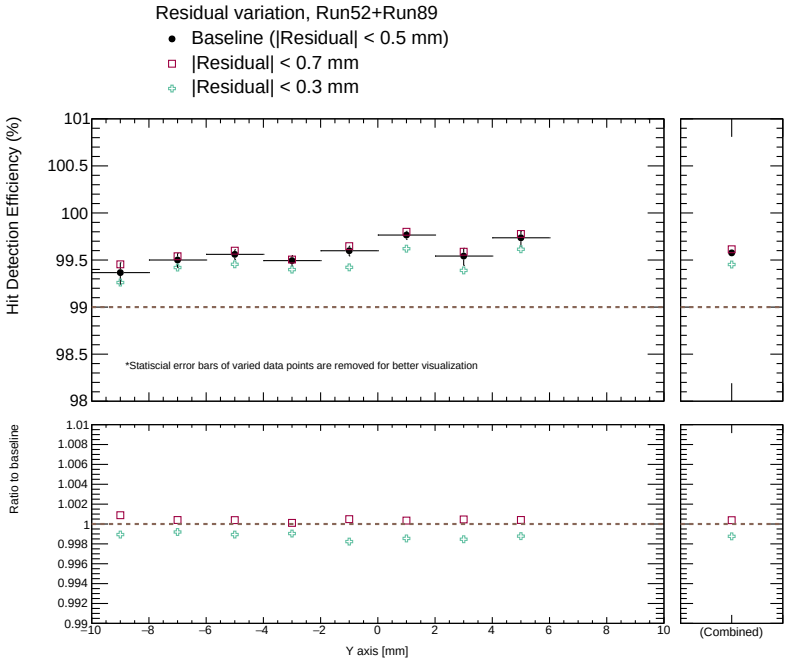


**Figure 24:** Ladder hit detection efficiency for different residual cuts for Run52 and Run89 combined. The right panel shows the result inclusive to the track position.

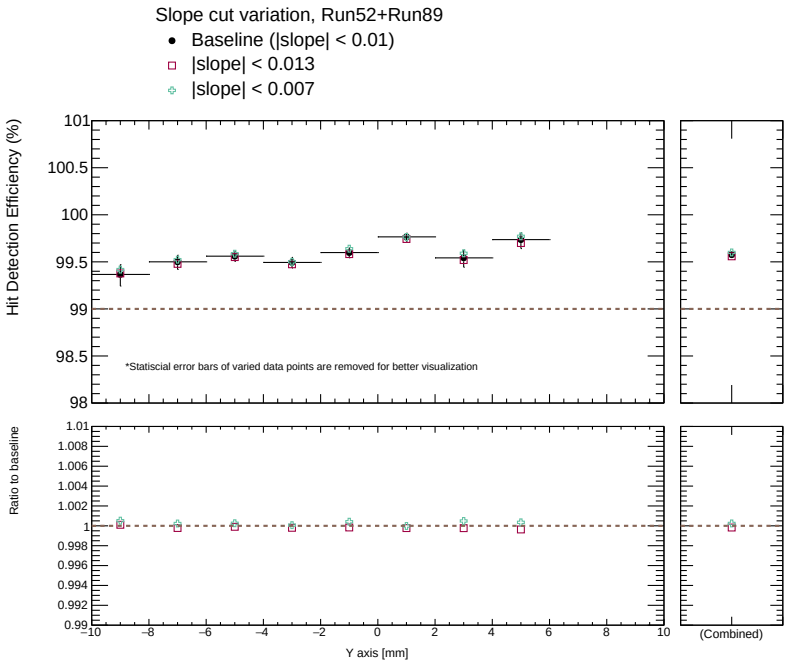


**Figure 25:** Ladder hit detection efficiency for different slope cuts for Run52 and Run89 combined. The right panel shows the result inclusive to the track position.

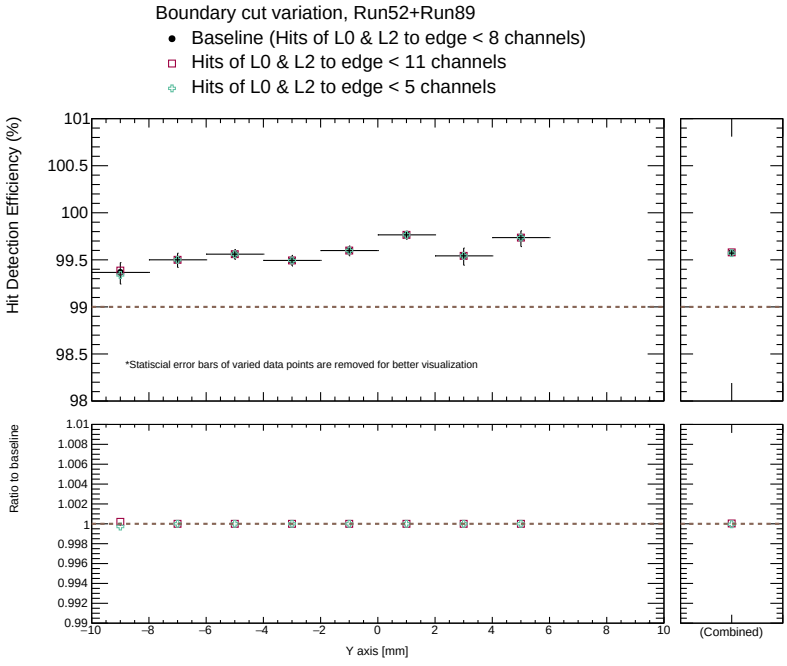


**Figure 26:** Ladder hit detection efficiency for different boundary cuts for Run52 and Run89 combined. The right panel shows the result inclusive to the track position.

The total systematic uncertainty in each bin is obtained using the same way as described above, as shown in Figure 27.

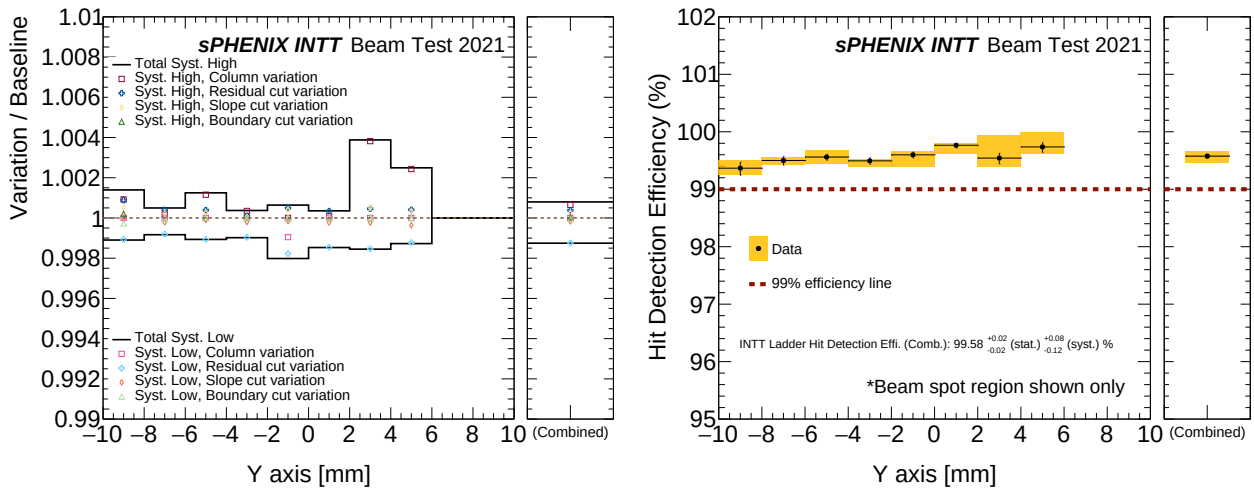


**Figure 27:** Total systematic uncertainty (left) and final measured INTT ladder hit detection efficiency (right) as a function of Y axis for Run52 and Run89 combined. The right panel of each plot shows the result inclusive to the track position. In the right plot, the vertical extent of each box represents the total systematic uncertainty, while the vertical line shows the statistical uncertainty.

And the final reported INTT ladder hit detection efficiency is

$$\text{Hit detection effi. of INTT} = 99.576\ ^{+0.021}_{-0.022}(stat.)\ ^{+0.079}_{-0.125}(syst.)\%. \tag{5}$$

# 6 Number of reconstructed track distribution

In this topic, Run64 is used. Before the Run64 data taking, there is one thin lead plate placed in between beam and INTT telescope. Since the positron beam was delivered, a little shower with multiple particles interacting with INTT ladders is expected. The data is analyzed to obtain the number of reconstructed track distribution, and compare with that of MC.

Since we are not measuring the detection efficiency, the method is different. The track is reconstructed by looping over all clusters in the three INTT ladders in each column. And the quality of each found combination is evaluated by fitting the three clusters with a slope line. The combination with the smallest reduced chi-square is checked. The residual (L1 - L2Lo interpolation) is required to be within 0.5 mm to be considered as good track. When a good track is found, the used three clusters are then removed from the cluster pool of each layer. And then we repeat the procedures, starting from looping over the clusters. Note that, single cluster can only be involved in one good track, while one column could have more than one reconstructed good track in one event. And in this analysis, all 13 columns of INTT half-ladder are checked.

In this analysis, events with clone hit are discarded. And since all 13 columns are used to obtain the maximal number of tracks, the alignment is the key correction. However, the beam spot is not wider enough to cover all 13 columns, as shown in Figure 16. We therefore use the fitting method to obtain the correction function. In each sensor type we select four columns with relatively higher statistics, and measure the individual L1 alignment with respect to Lo and L2, as shown in

Figure 28. The slope lines are then extrapolated to all columns in the half-ladder. In the other words, each column has its corresponding l1 alignment correction. Based on the slopes, the ladder L1 is slightly tilted in the Z axis (beam direction) with respect to L0 and L2. In simulation, there is no L1 rotation. The correction for all columns is given by the average of L1 alignment corrections measured by column U9, U10 and U11 (the beam spot region).

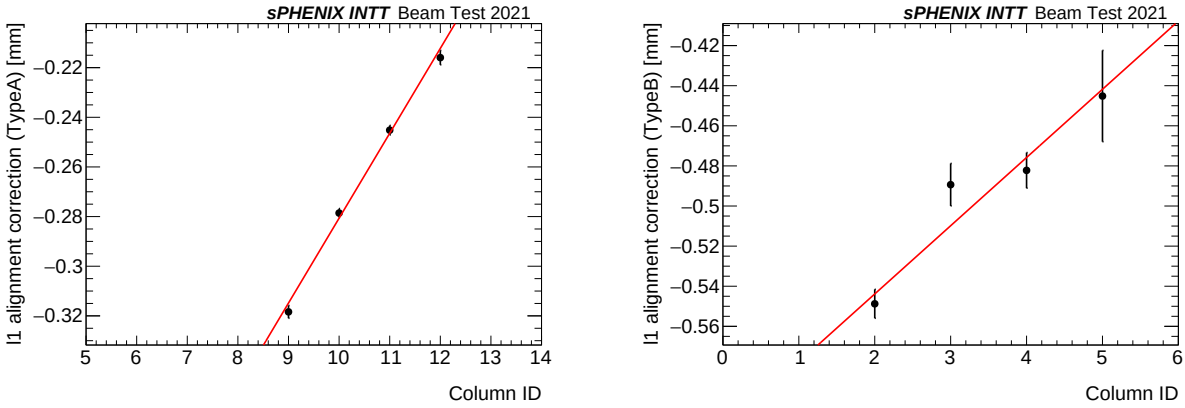


**Figure 28:** L1 alignment correction as a function of Column ID for Type A (left) and Type B (right) sensors. Type A sensor covers column U6 to U13, while the Type B sensor covers column U1 to U5.

In data Run64, there are two hot channels in L2, as shown in Figure 29.

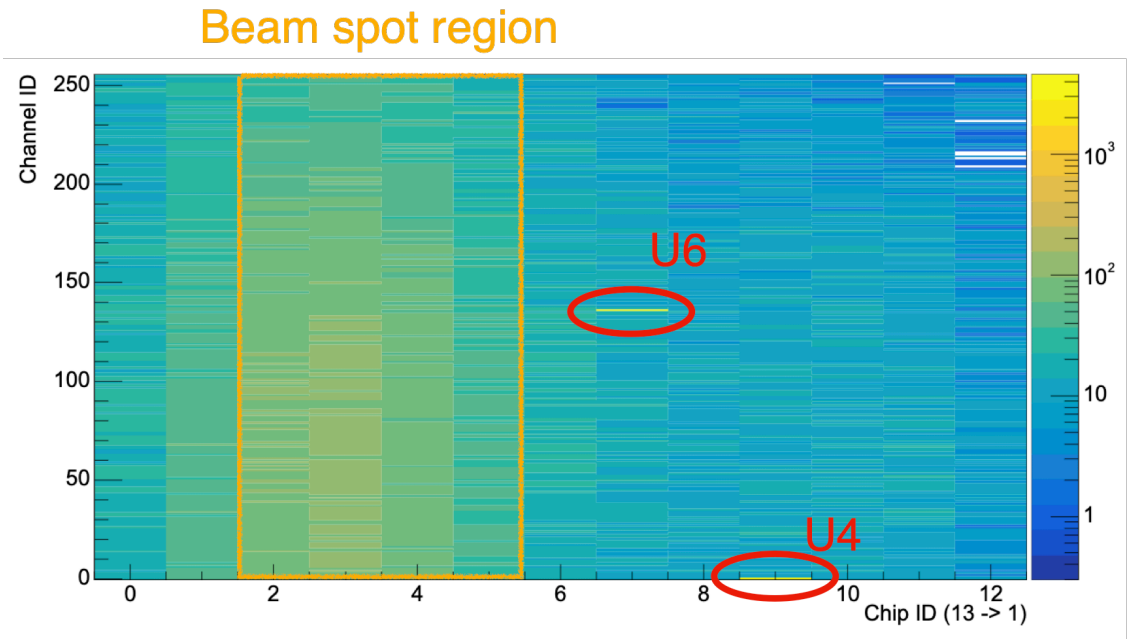


**Figure 29:** Hit map of data Run64 L2. Two hot channels are found, one in column U4 and one in column U6. In order to follow the actual ladder geometry, the 2D histogram is plotted in the way that the rightmost column is column U1.

The number of reconstructed tracks distributions with and without rejecting columns U4 and U6 are shown in Figure 30. The two distributions are basically identical, and agree with simulation within the statistical uncertainties, indicating a very robust noise hit rejection by the 3-hit tracking. Figure 31 shows the reconstructed track distribution without rejecting columns U4 and U6.

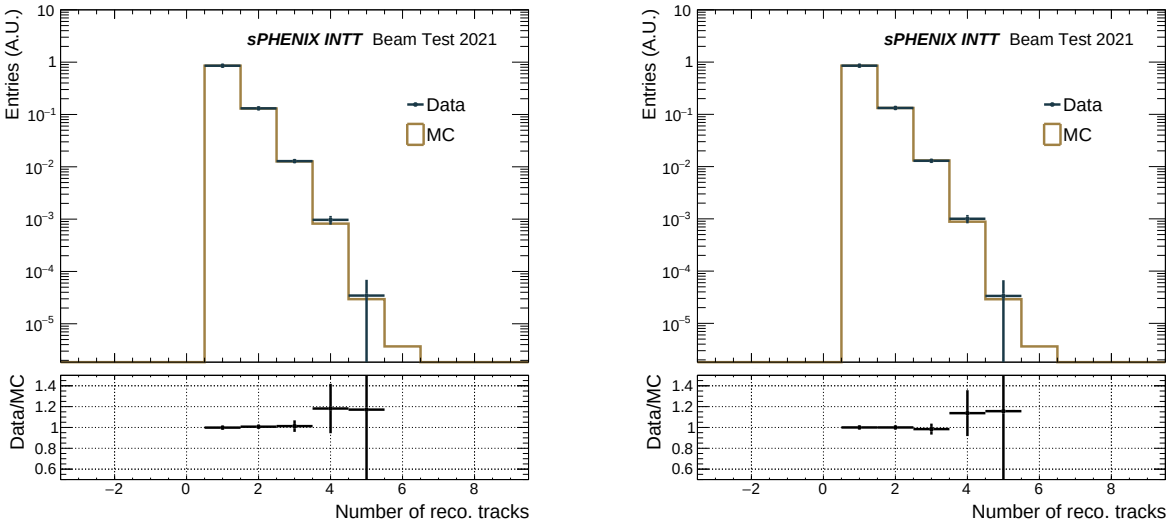


**Figure 30:** Number of reconstructed tracks distribution with (left) and without (right) rejecting columns U4 and U6.

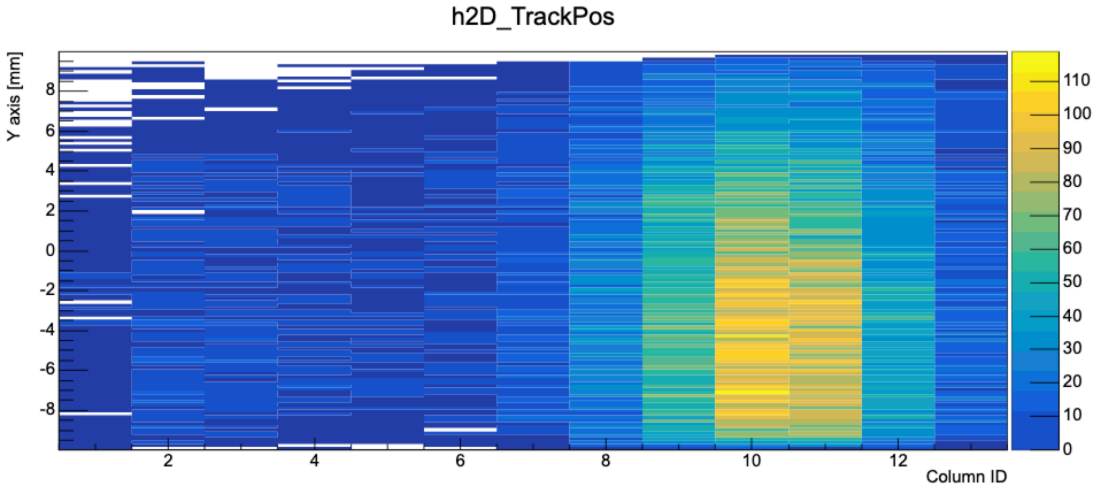


**Figure 31:** Reconstructed track position distribution without rejecting columns U4 and U6, to emphasize the robustness of the noise suppressing by the 3-hit tracking. In this plot, the coordination in the X axis is opposite to that of Figure 29. The column U1 is located at the leftmost column.

## References

[1] (Particle Data Group Collaboration). Review of particle physics. *Progress of Theoretical and Experimental Physics*, 2020(8):083C01, 08 2020. arXiv:https://academic.oup.com/ptep/article-pdf/2020/8/083C01/34673722/ptaa104.pdf, doi:10.1093/ptep/ptaa104. 3

# Appendices

## A Beam Test 2019

- Data log of beam test 2019:
  - https://docs.google.com/spreadsheets/d/1dekFg1BBAFC47S50X1B7xyGoxaxvmTAin9GgqodQBwU/edit#gid=0.
- Some of the data can be found in NCUHEP CHiP server: /home/cwshih/sPHENIX/INTT/Testbeam/Testbeam2019/INTT_2019_testbeam.